Monthly Notices
of the
ROYAL ASTRONOMICAL SOCIETY

MNRAS **446,** 627–632 (2015) doi:10.1093/mnras/stu2071

Experimental validation of Lyot stop apodization in ground-based coronagraphy

Miguel A. Cagigas,[1⋆] Pedro J. Valle,[1] Manuel P. Cagigal,[1] Xesús Prieto-Blanco,[2] Antonio Pérez-Garrido,[3] Isidro Villo-Pérez,[4] B. Femenía,[5] J. A. Pérez-Prieto,[5] L. F. Rodríguez,[5] R. López,[5] A. Oscoz[5] and R. Rebolo[5]

[1]*Departamento de Física Aplicada, Universidad de Cantabria Avenida de los Castros s/n, E-39005 Santander, Spain*
[2]*Facultade de Óptica e Optometría, Campus Vida, E-15782 Santiago de Compostela, Spain*
[3]*Dpto. Física Aplicada, Universidad Politécnica de Cartagena, Campus Muralla del Mar, E-30202 Cartagena, Murcia, Spain*
[4]*Dpto. Eléctronica, Universidad Politécnica de Cartagena, Campus Muralla del Mar, E-30202 Cartagena, Murcia, Spain*
[5]*Instituto de Astrofísica de Canarias, C/ Vía Láctea S/N, E-38200 La Laguna, Spain*

Accepted 2014 October 1. Received 2014 October 1; in original form 2014 April 13

ABSTRACT

We show that the use of apodizing functions at the coronagraph Lyot plane may be useful for improving the image contrast of ground-based coronagraphs. An experimental set-up consisting of a tip–tilt mirror, a coronagraph and a low-noise EMCCD camera was implemented at the William Herschel Telescope. Images were taken in the *I* band, which meant that the D/r_0 value was around 10. Experimental results confirm that, for moderately aberrated wavefronts, our instrument works as theoretically expected, and that the contrast value attained is high enough to provide direct detection of faint companions.

Key words: instrumentation: high angular resolution – stars: imaging.

1 INTRODUCTION

Since 1978, when Harris (1978) published an extensive review of apodizing functions for improving signal detectability, pupil apodization has found applications in such varied fields as data storage (Canales et al. 2009), beam reshaping (Dickey & Holswade 2000) and confocal microscopy (Canales et al. 2006). In particular, we are interested in pupil apodization for high-contrast imaging of astronomical objects with ground-based telescopes. Most apodizing functions have been developed for ideal systems; that is, for dealing with non-aberrated wavefronts. In this case, the best option is to apodize the telescope pupil entrance, since this has been demonstrated both theoretically and experimentally (Guyon 2003). However, considerable effort is being devoted to making ground-based observation of exoplanets a realistic option (e.g. Soummer et al. 2011). In particular, the technique based on the local suppression of stellar haloes (Codona & Angel 2004) seems to be a clear solution for dealing with atmospherically distorted wavefronts. An extended review of state-of-the-art ground-based coronagraphy was published by Mawet et al. (2012).

In a previous article (Cagigas, Valle & Cagigal 2013), we explored the use of super-Gaussian (SG) apodizing functions in both the entrance pupil of the telescope and the Lyot stop plane of a coronagraph. We selected SG functions not only because they are easy to study analytically but also because they provide a good balance between absorbed energy and contrast. We restricted our analysis to ground-based telescopes in which the condition $D/r_0 < 7.8$ is fulfilled, where D is the pupil diameter and r_0 the Fried parameter. This condition ensured the coherent energy of the stellar point spread function (PSF) was larger than the incoherent one.

We have recently carried out an experimental test of an instrument consisting of a coronagraph combined with a tip–tilt mirror, two low-noise Andor EMCCD cameras and a software package to select the best frames. *I*-band observations were performed at the 4.2-m William Herschel Telescope (WHT). This means that the condition $D/r_0 < 7.8$ was extremely difficult to reach, and that the incoherent energy of the stellar PSF was larger than the coherent one.

The goal of this paper is to use computer simulations to find out whether apodization is more effective when placed at the pupil entrance plane or at the Lyot stop plane in conditions where the D/r_0 value is above or below the threshold $D/r_0 < 7.8$. We also checked experimentally whether proper Lyot apodization combined with a lucky image detection system would allow the coronagraph to reach a contrast level high enough to make the technique useful for ground-based telescopes.

In Section 2 we describe SG functions as the two-dimensional convolution of hard-edged (HE) circular and Gaussian functions. In Section 3 we estimate the effects on coronagraphic images of using a SG apodizing profile at the telescope entrance pupil or at the Lyot

⋆E-mail: miguelcagigasga@gmail.com

stop. Section 4 shows the procedure followed to obtain filters with a SG transmittance profile. The experimental coronagraphic set-up is sketched in Section 5 whilst experimental results are shown in Section 6. Section 7 shows the result of observing the binary star HD 112196. Finally, Section 8 summarizes the most important results obtained in the study.

2 SUPER-GAUSSIAN PUPIL FUNCTIONS

The nth-order two-dimensional normalized SG function is defined as:

$$\mathrm{SG}(n, r) = \mathrm{e}^{-\left|\frac{r}{\sigma}\right|^n} \tag{1}$$

where σ is the half-width and r is the usual radial coordinate. It can be shown that the SG function ranges from a Gaussian function for $n = 2$ to a HE circle (a HE circle is a function having unit value inside the circle and zero value outside). In this paper we will always take $n = 4$.

The $\mathrm{SG}(n, r)$ radial functions can be seen as the two-dimensional convolution of a HE circle and a Gaussian radial function $G(r)$ (Cagigas et al. 2013). The width and order of the resulting SG function will only depend on the ratio of the Gaussian width and HE circle diameter. Assuming the SG function to be the result of a convolution product, its Fourier transform will be the product of the individual Fourier transforms:

$$\mathrm{SG}(n, r) = \mathrm{HE}(r) \otimes G(r) \xrightarrow{\mathrm{FT}} \mathrm{sg}(\omega) = A(\omega) \cdot g(\omega), \tag{2}$$

where $A(\omega)$ is the Fourier transform of the HE circle function (its square modulus $|A(\omega)|^2$ is the well-known Airy pattern) and $g(\omega)$ the Gaussian function resulting from the Fourier transformation of $G(r)$.

A detailed analysis of the apodizing properties of the SG functions and a comparison with prolate spheroid apodizing functions has already been carried out (Cagigas et al. 2013). It was found that while a prolate spheroidal pupil apodizer results in a better inner working angle, the SG pupil produces a larger throughput and the same diffraction rings for angular distances larger than $9\lambda/D$. It is important to notice that, when dealing with distorted atmospheric wavefronts, the coronagraphic mask needs to have an angular radius of several diffraction rings to provide good contrast. Hence, under these conditions, it seems to be more advantageous to use SG apodizing functions for detection at large angular distances.

3 APODIZED CORONAGRAPHY

For a ground-based telescope, the PSF is composed of a coherent peak and a surrounding speckled halo (Cagigal & Canales 2000). It can be shown that the coherent energy in the PSF is higher than the incoherent one when $D/r_0 < 7.8$, where D is the telescope entrance pupil diameter and r_0 the atmospheric Fried parameter (Hardy 1998). Since apodization affects only the coherent energy, we expect that the effect of apodization will decrease when D/r_0 increases, becoming almost negligible for D/r_0 values much greater than 7.8.

In a recent paper (Cagigas et al. 2013), we studied the detectability improvement produced when SG apodizing functions were used for a ground-based coronagraph. We compared the results of using a SG apodizing profile at the telescope entrance pupil and only at the Lyot stop for $D/r_0 < 7.8$.

We used the computer simulation described by Cagigas et al. (2013) to analyse the effect of apodization on the contrast curves of the instrument. Simulations for $D/r_0 = 5$ and $D/r_0 = 10$ are shown in Fig. 1. It can be seen that the pupil apodization for $D/r_0 = 5$ performs slightly better than the unapodized pupil, but this advantage almost disappears for $D/r_0 = 10$. However, the Lyot stop apodization increases the contrast in both cases, which is particularly interesting for high D/r_0 values.

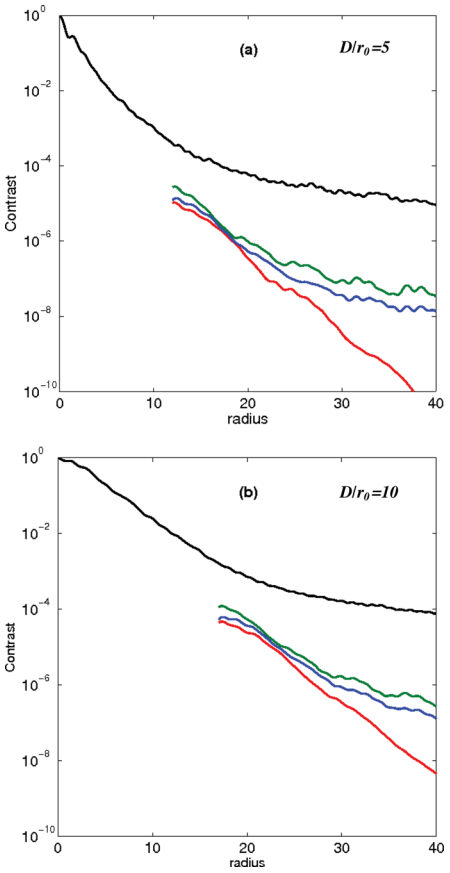

Figure 1. Contrast curves for an unapodized pupil, no coronagraphic masks and HE Lyot (black curve), HE coronagraphic masks and HE Lyot (green curve), SG apodized pupil, HE coronagraphic masks and HE Lyot stop (blue curve) and unapodized pupil, and HE coronagraphic masks and SG Lyot stop (red curve). For $D/r_0 = 5$ (a) the HE coronagraphic mask radius was $12\lambda/D$ and for $D/r_0 = 10$ (b) the HE coronagraphic mask radius was $17\lambda/D$.

4 DESIGN AND MANUFACTURE OF A SUPER-GAUSSIAN LYOT STOP

4.1 Stop design

Given the difficulty of manufacturing a SG mask profile, we used a half-tone dot process to reproduce it. The microdot technique has already been analysed (Martinez et al. 2009a, 2009b) and has been developed for the *James Webb Space Telescope* NIRCam coronagraph (Krist et al. 2009). These masks consist of distributions of opaque square pixels (called dots) to reproduce the continuous transmission of a filter and they have several advantages: relative ease of manufacture, achromaticity, reproducibility and the ability to generate continuous transmission ranges without introducing wavefront errors. A detailed description of the design process can be found in Martinez, Dorrer & Kasper (2009c).

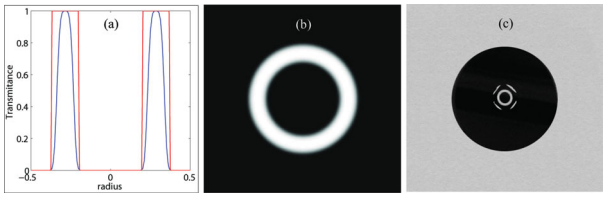

Figure 2. (a) HE and SG mask profiles, (b) binary SG Lyot stop and (c) manufactured binary SG Lyot stop.

4.2 Stop manufacture

The Lyot stop was fabricated by lithographic methods with commercial photographic optics. The process was carried out in two stages, resulting in an intermediate and a final mask, both comprising a patterned chromium layer on a flat glass substrate. First, the glass substrates were coated with a chromium layer 0.3 μm thick in a high-vacuum deposition chamber, and then a photoresist layer was spun on the chromium.

Since the coronagraph was planned to be mounted on the WHT, the Lyot stop has to block not only the light diffracted by the telescope pupil but also that diffracted by the central obscuration. Fig. 2(a) shows transversal cuts of the transmittance function corresponding to the HE and SG Lyot stops used at the WHT. In particular, the SG Lyot stop, as shown in Fig. 2(b), has a size of 928 × 928 pixels, and the pixel size is 250 μm.

The pattern, consisting of a square binarized mask of side 928 pixels, was printed with a size of 232 × 232 mm. A first photoreduction was carried out in a Linhof enlarger provided with a Rodenstock Apo-Rodagon-N 1:2.8/50-mm lens, set at optimum magnification (−0.1×) and $f/4$. The image was used to directly expose one photoresist-coated substrate for 2 h while the original was being illuminated with four commercial Hg lamps (125 W each). The intermediate mask was completed after development of the photoresist, etching of the chromium layer and removal of the residual photoresist. This mask was used as an object to expose a new coated substrate in a second photoreduction step. This time a Canon MP-E 65-mm 1-5× Macro Lens in reversed configuration was used to achieve a −0.2× magnification at an effective f-ratio of 4.2. Moreover, the object was illuminated by transmission through an optical system which filters the g line (436 nm) from a mercury lamp and provides partial spatial coherence that slightly improves the resolution. The exposure lasted 35 min, whereas the development and etching were similar to that of the intermediate mask. The final mask has a 4.64 mm side and a pixel size of 5 μm. One of the Lyot stops produced is shown in Fig. 2(c). It can be seen that four slits appear surrounding the stop as a result of the manufacturing process. These slits were conveniently covered and an antireflective layer of 850 nm was deposited on both faces of the stop.

5 EXPERIMENTAL SET-UP

The coronagraph design is fully reflective and thus achromatic. The functionality comes in two stages. The first stage (see Fig. 3) scales the nominal (telescope) focal plane FP1, 20 times to provide a second focal plane, FP2, where the occulting mask will be placed. One off-axis parabolic mirror (OAP1, fOAP = 25 mm) and a spherical mirror (SPHE1, fSPHE1 = 500 mm) are used to provide the required scale. A commercial piezo tip–tilt (T-T) mirror from Physik Instrumente has been placed between OAP1 and SPHE1 to compensate for small star movements. The second stage follows a collimator-camera configuration while supplying a pupil image

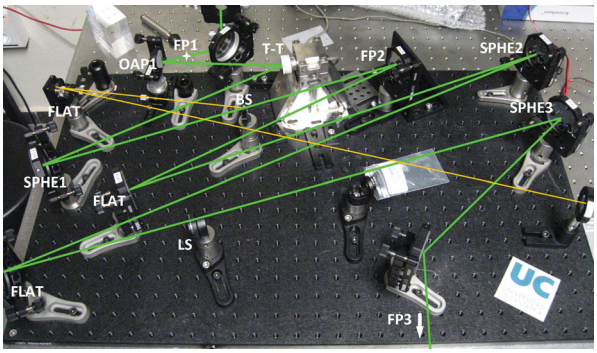

Figure 3. Coronagraph layout. FP1: telescope focal plane; OAP1: off-axis parabolic mirror; T-T: tip–tilt mirror; SPHE1, 2, 3: spherical mirrors; FP2: scaled focal plane and coronagraphic mask; LS: Lyot stop; FP3: detector focal plane.

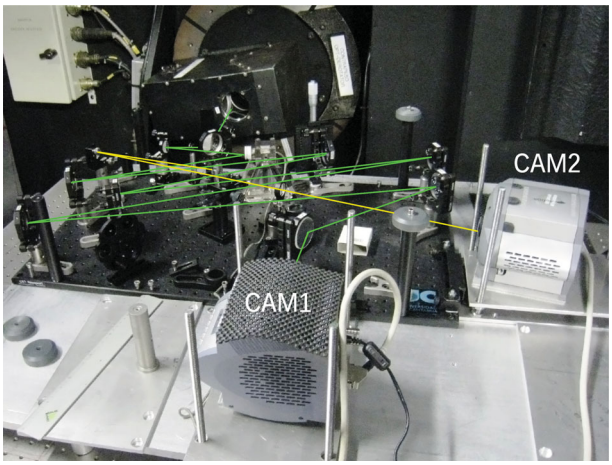

Figure 4. Coronagraph layout. The lucky imaging acquisition system FASTCAM (CAM1), the tip–tilt control camera (CAM2) and the coronagraph placed at the WHT Nasmyth focus table can be seen.

of the system. The pupil is placed at the focal plane of SPHE2 (fSPHE2 = 1000 mm) whilst the camera is at the image focal plane of SPHE3 (fSPHE3 = 500 mm). The Lyot stop is located 500 mm before SPHE3. The powered mirrors are spherical because of the long working focal length of the system. The long distance between SPHE1 and SPHE2 is needed to provide a minimum pupil size of 5 mm in this case. As a result of this restriction, several flat packaging mirrors were used in the final assembly.

Fig. 4 shows the final set-up. The coronagraph shown in Fig. 3 is now feeding the Andor scientific camera (CAM1). The orientation of the tip–tilt mirror is driven in a closed-loop control mode. There are two applied voltages in the system, one per axis. Images of the star acquired by CAM2 (yellow paths in Figs 3 and 4) are employed as feedback for the closed loop. The control is performed by a simple digital PID controller with a governing equation given by:

$$V_n = V_{n-1} + K_p e_n + K_d\,[e_n - e_{n-1}] + K_i\,[e_n + e_{n-1}]\,, \qquad (3)$$

where V_n is the applied voltage to the tip–tilt mirror at step n, K_p, K_d and K_i are constants, and e_n (e_{n-1}) is the positional difference between an initial set point and the centroid of the star at step n ($n-1$).

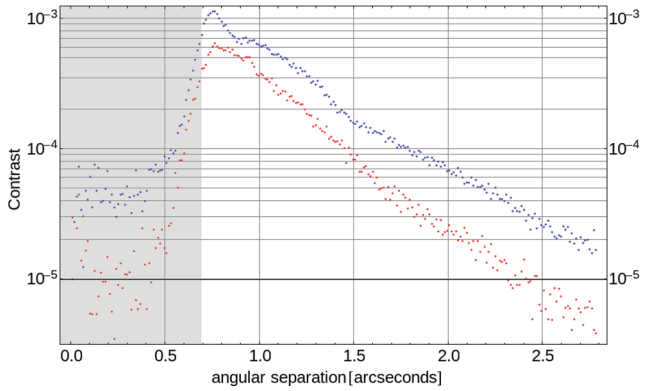

Figure 5. Experimental contrast curves as a function of angular distance to the mask centre obtained by the set-up shown in Fig. 4. The behaviour is as theoretically predicted (see Fig. 1). The HE Lyot stop is shown in blue and the SG Lyot stop in red.

6 EXPERIMENTAL RESULTS

The coronagraph described in the previous section was tested at the WHT. First, we took observations of the bright star HR 622 in the *I* band in December 2012. At the moments of best seeing, we were detecting under $D/r_0 \simeq 10$. The coronagraph, consisting of an unapodized pupil, HE coronagraphic masks and a HE or SG Lyot stop, was completed with an S-330 piezo tip–tilt mirror from Physik Instrumente.

To freeze the atmospherically induced distortions, the exposure time used in the scientific camera (CAM1, Fig. 4) was 30 ms. In this camera 4×4 binning was applied to get images of 256×256 pixels with an angular size of 23.2 mas/pixel.

To check the performance of the SG Lyot stop, eight cubes of 10 000 frames were taken and stored using an HE Lyot stop and four cubes of 10 000 frames using an SG Lyot stop. We selected the frames with the greatest contrast, corresponding to a lower D/r_0 value, for both Lyot types. We took the images with the lowest total intensity for both kinds of Lyot stops and, after cancelling the static background, averaged the radial intensity.

Fig. 5 shows the transversal cut of the averaged contrast experimentally obtained for the object HR 622 as a function of the angular distance to the star's position. We used a coronagraphic set-up with an unapodized pupil and a HE coronagraphic mask covering an angular distance corresponding to 17 stellar diffraction rings. In one curve, a HE Lyot stop reducing the telescope pupil diameter to 80 per cent of its initial size was used, while an SG Lyot stop, whose profile is shown in Fig. 2(a) (red line), was used for obtaining the other one.

The first conclusion is that the SG Lyot stop slightly improves the HE performance at the mask border, but the difference increases with angular distance. On the other hand, a contrast greater than 10^3 is reached in the coronagraphic mask border, and this contrast can increase up to 10^5 for distances around 2.5 arcsec. These contrast values could be improved by properly averaging the image over a set of short exposure images. However, to determine the performance limit of the set-up, it is more exact to show the result corresponding to the image with the lowest D/r_0, since the contrast improvement due to the average might be lost when using images with higher D/r_0 values. A further contrast improvement could be attained by applying the angular differential imaging technique, but once again frames with higher D/r_0 values would be necessary.

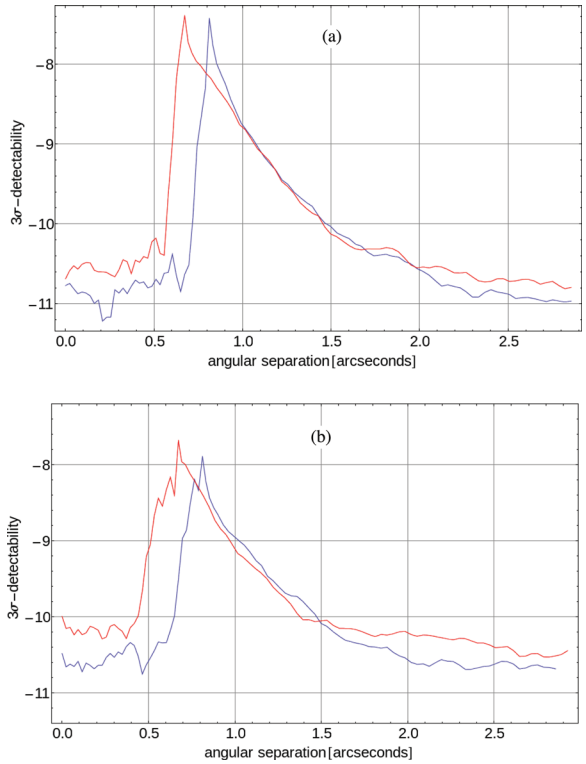

Figure 6. (a) Comparison between the experimental results obtained for a coronagraphic mask covering 17 star diffraction rings (red line) and those obtained from a mask covering 22 star diffraction rings (blue line) using a HE Lyot stop. (b) The same curves when an SG Lyot stop is used.

If we compare the curves in Fig. 5 with those theoretically predicted, as shown in Fig. 1(b), where both sets were obtained for $D/r_0 = 10$, we see that the behaviour of the experimental curves is that expected for both the HE and the SG Lyot stops. The relative distance is also reproduced by the experiment as a function of angular distance. However, experimental contrast values are about half an order of magnitude higher than those theoretically expected.

To compare the performances of different masks and Lyot stops, we defined the 3σ detectability as:

$$3\sigma \text{ detectability} = -2.5 \log \left(\frac{\text{Peak}}{3\sigma(r)} \right), \tag{4}$$

where Peak is the peak intensity of the stellar companion and $\sigma(r)$ is the standard deviation as a function of the angular distance to the star's position. Fig. 6 shows 3σ detectability curves obtained from a set of 375 frames corresponding to the darkest 5 per cent of the total number of frames. Comparison between the experimental results obtained for a coronagraphic mask covering 17 star diffraction rings and those obtained from a mask covering 22 star diffraction rings is shown in Fig. 6(a) when using the previously described HE Lyot stop. Fig. 6(b) shows curves for the same set-up when the SG Lyot stop was used.

It is necessary to state that the peaks in the curves of Fig. 6 correspond to the coronagraphic mask border position; hence, a companion can be detected only when it is located to the right of a peak. Fig. 6(a) shows that the curve slope is the same for both coronagraphic masks, as expected, and that the small mask allows detection at smaller angular distances than the large mask. Fig. 6(b) shows, besides the earlier detection from the small mask, that the use of the SG Lyot stop reduces the 3σ detectability for distances

between 0.8 and 1 arcsec, but for greater distances the performance of both the HE and the SG Lyot stops tends to equalize. In all cases, a companion 10 magnitudes fainter than the parent star can be detected at a distance of 1.5 arcsec.

7 OBSERVATION OF THE BINARY STAR HD 112196

During this campaign, several binary stars with close high-contrast companions were observed. One of these, HD 112196, is an F8V star at 34 pc with a known companion discovered by Metchev & Hillenbrand (2009) using adaptive optics on the 5-m Hale Telescope. According to their observations in the K_s band (2190 nm), the companion, at 1.6 arcsec from the primary, has a visual magnitude of 7.8, implying a mass of 0.59 $M_\odot$ from the theoretical models of Baraffe et al. (1998). More recently, Roberts et al. (2012) performed infrared spectroscopy of HD 112196 B, estimating a spectral type of M2–M3 as the best fit to the models.

HD 112196 was observed in the *I* band (807 nm) with a four-binning configuration and 40-ms exposure time using the median mask. A selection of the best 100 frames from a total of 1500 was used to create an averaged image, and each frame was re-centred using the brightest speckles of the star (Fig. 7). Finally, a wavelet filter was used. To obtain the magnitude, we performed aperture photometry on the companion, calibrating it with unmasked images of HD 77407 ($I = 6.4$) and HD 71881 ($I = 6.7$), obtained using the same technique and observational parameters, and correcting only for the exposure time, which was 35 ms. The measured magnitude is $I = 9.9 \pm 0.1$, giving an absolute magnitude of $M_I = 7.3 \pm 0.2$ using a parallax of 29.54 ± 1.0 mas from *Hipparcos* (Van Leeuwen 2007). The resulting $I - K_s$ colour is 2.13 ± 0.23.

Comparison of both the absolute magnitude and the $I - K_s$ colour with the theoretical models of Baraffe et al. (1998) – see Fig. 8 – suggests a mass of 0.57 $M_\odot$, which is compatible with the M2–M3 spectral type obtained by Roberts et al. (2012) and with the mass obtained by Metchev & Hillenbrand (2009) using K_s. Also, HD 112196 B shows a very similar magnitude and colour to those of several M2-type standard stars, such as Gl 507.1, Gl844 and Gl 649 (Jenkins et al. 2009).

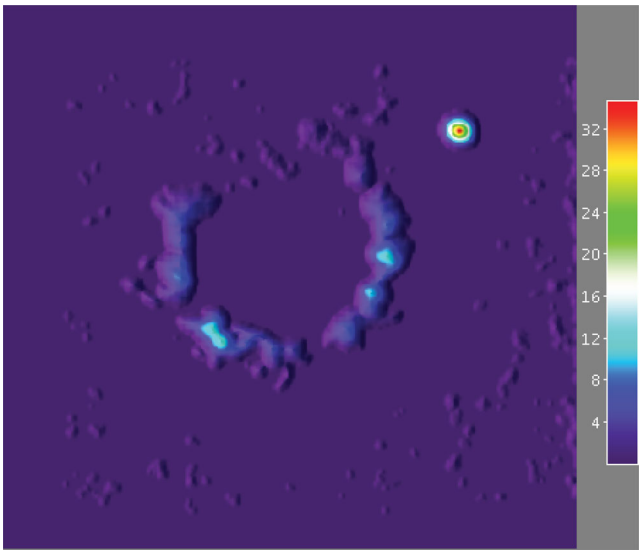

Figure 7. Processed image of HD 112196 in the *I* band with the primary masked showing the companion at 1.6 arcsec. The image is an average of the best 100 frames, with a 40-ms exposure time.

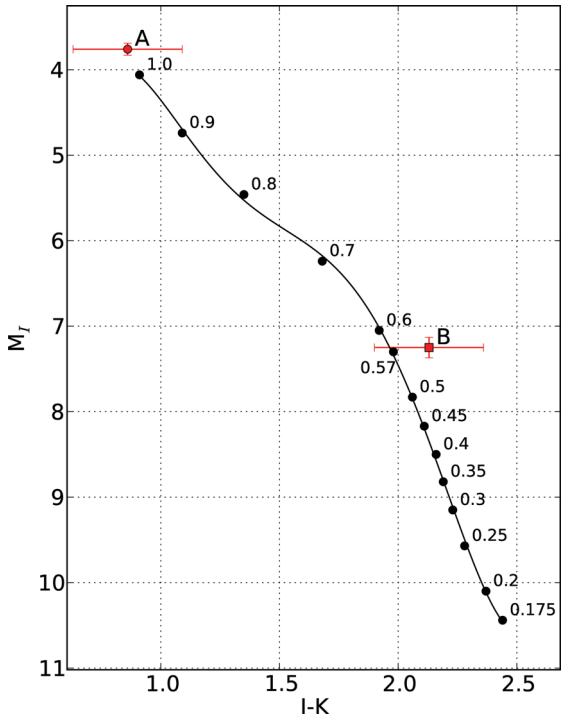

Figure 8. Absolute magnitude–colour diagram of HD 112196 superimposed on the theoretical models of Baraffe et al. (1998). Corresponding masses in the model are indicated in solar masses. HD 112196 B is seen to be quite compatible with an M2-type star.

8 CONCLUSIONS

A theoretical analysis of the effect of apodizing functions has been carried out by comparing the effect of separately apodizing the entrance pupil and the Lyot stop plane of a coronagraph. The resulting contrast curves show that for moderate aberration (D/r_0 around 7.8), Lyot stop apodization produces higher contrast.

An experimental set-up consisting of a coronagraph, a tip–tilt mirror and a low-noise EMCCD camera was implemented at the WHT. The set-up was used to check that Lyot stop apodization is an effective way of reducing starlight noise and also to show that the whole instrument is able to attain a contrast value up to 10^6 for an angular distance of 2 arcsec. This contrast value, fairly modest for space-based detection, is really competitive for ground-based mid-sized telescopes at the far-red (*I* band) optical part of the spectrum and could be improved by standard post-processing techniques.

ACKNOWLEDGEMENTS

This research was supported by the Ministerio de Economía y Competitividad under project FIS2012-31079 and the Fundación Séneca of Murcia under projects 15419/PI/10 and 15345/PI/10. We would like to thank the staff at Fractal S.L. for their help during the design of the coronagraph.

REFERENCES

Baraffe I., Chabrier G., Allard F., Hauschildt P. H., 1998, A&A, 337, 403
Cagigal M. P., Canales V. F., 2000, J. Opt. Soc. America A, 17, 903

Cagigas M. A., Valle P. J., Cagigal M. P., 2013, Opt. Express, 21, 12744
Canales V. F., Cagigal M. P., 2006, Opt. Express, 14, 10393
Canales V. F., Valle P. J., Oti J. E., Cagigal M. P., 2009, Chinese Opt. Lett., 7, 720
Codona J. L., Angel R., 2004, ApJ, 604, L117
Dickey F. M., Holswade S. C., 2000, Laser Beam Shaping: Theory and Techniques. Marcel Dekker Inc., New York
Guyon O., 2003, A&A, 404, 379
Hardy J. W., 1998, Adaptive Optics for Astronomical Telescopes. Oxford University, New York
Harris F. J., 1978, Proc. IEEE, 66, 51
Jenkins J. S., Ramsey L. W., Jones H. R. A., Pavlenko Y., Gallardo J., Barnes J. R., Pinfield D. J., 2009, ApJ, 704, 975
Krist J. E. et al., 2009, Proc. SPIE, 7440, 74400W
Martinez P. et al., 2009a, A&A, 495, 363
Martinez P., Dorrer C., Kasper M., Dohlen A. B., 2009b, A&A, 500, 1281
Martinez P., Dorrer C., Kasper M., 2009c, A&A, 705, 1637
Mawet D. et al., 2012, Review of small-angle coronagraphic techniques in the wake of ground-based second-generation adaptive optics systems, http://arxiv.org/abs/1207.5481
Metchev S. A., Hillenbrand L. A., 2009, ApJS, 181, 62
Roberts L. C., Jr et al., 2012, AJ, 144, 14
Soummer R., Sivaramakrishnan A., Pueyo L., Macintosh B., Oppenheimer B. R., 2011, ApJ, 729, 144
Van Leeuwen F., 2007, A&A, 474, 653

This paper has been typeset from a TEX/LATEX file prepared by the author.